

Contents lists available at ScienceDirect

Journal of Aerosol Science

journal homepage: www.elsevier.com/locate/jaerosci





The fractal characteristics of atmospheric coated soot: Implication for morphological analysis

Jie Luo ^a, Qixing Zhang ^{a,*}, Chenchong Zhang ^b, Yongming Zhang ^a, Rajan K. Chakrabarty ^{b,c}

- ^a State Key Laboratory of Fire Science, University of Science and Technology of China, Hefei, Anhui 230026, China
- ^b Center for Aerosol Science and Engineering, Department of Energy, Environmental and Chemical Engineering, Washington University in St. Louis, St. Louis, MO 63130, USA
- ^c McDonnell Center for the Space Sciences, Washington University in St. Louis, St. Louis, MO 63130, USA

ARTICLE INFO

Editor: Dr. Chris Hogan

Keywords: Soot Fractal characteristics Morphology Coating

ABSTRACT

In this work, we have numerically investigated the variation of fractal characteristics of soot particles as soot is coated. We found that the ideal fractal law can fit the morphologies of coated soot only when the radius of gyration (R_g) of coated soot is identical to that of the soot core. In that case, the fractal dimension (D_f) of coated soot is close to that of the soot core, which can explain why the unchanged fractal dimension was observed by the previous study as soot was evenly coated. As the voids among monomers is commonly filled firstly, the R_g of coated soot obtained from the two-dimensional (2D) method would be close to that of the soot core, so the measured fractal dimension would be close to that of the soot core. Our results also show that the fractal parameters of coated soot at different size scales can be varied, so the ideal fractal law is difficult to fit the structures of unevenly coated soot universally. Besides, we also found that the effective fractal dimension can increase as soot is unevenly coated. The results of the Q-space analysis show that as soot particles are unevenly coated, the power-law exponent of the structure factor (S(q)) versus the scattering wave vector (q) tends to -4 for heavily coated soot. This means that heavily, unevenly coated soot exhibits the characteristics of nearly spherical particles.

1. Introduction

Soot particles, as a major light absorber in the atmosphere, contribute great positive radiative effects to the climate. Soot has been evaluated to be the second largest anthropogenic contributor to global warming after CO₂ (Bond et al., 2013; Forster et al., 2007; Schwarz et al., 2008). Besides, soot can deposit on the snow and ice to lower the snow and ice albedo (Chỳlek, Ramaswamy, & Srivastava, 1983; He et al., 2018; Warren, 1982). The radiative effects of soot have gained increasing interest in recent years, while there are still large uncertainties. A cause of the uncertainties is the complex morphologies of soot. Many modeling studies have shown that various soot morphologies can lead to large uncertainties in the estimations of radiative properties (Adachi, Chung, & Buseck, 2010; Chakrabarty et al., 2007; Liu, Li, Yin, Zhu, & Feng, 2017; Liu & Mishchenko, 2005; Liu et al., 2020; Luo et al., 2019; Mishchenko, Dlugach, & Liu, 2016), while the morphological characteristics of soot, especially for coated soot, are still not fully understood.

https://doi.org/10.1016/j.jaerosci.2021.105804

^{*} Corresponding author.

E-mail address: qixing@ustc.edu.cn (Q. Zhang).

Freshly emitted soot aggregates are widely recognized to be composed of tens to hundreds of small spherules, and their structures can be well fitted by the fractal law. Given the monomer number (N_s), monomer radius (a), fractal prefactor (k_0), fractal dimension (D_f) and the radius of gyration (R_s), the fractal law can be described as (Forrest & Witten, 1979; Meakin, 1987; Sorensen, 2001):

$$N_s = k_0 \left(\frac{R_g}{a}\right)^{D_f} \tag{1}$$

where

$$R_g^2 = \frac{1}{N_s} \sum_{i=1}^{N_s} l_i^2 \tag{2}$$

where l_i represents the distance from the center of the *i*th monomer to the center of the aggregate. For the fractal soot, D_f can reflect the space-filling characteristic, while k_0 can be significantly affected by the shape anisotropy (stringiness) and monomer packing density (Heinson, Sorensen, & Chakrabarti, 2010; Lapuerta, Martos, & Martín-González, 2010; Sorensen & Roberts, 1997).

Two methods were commonly used to analyze the fractal parameters of soot aggregates. One of the methods is based on the threedimensional (3D) object reconstructed using the 3D electron tomography method. By exploring the 3D electron tomography method, average D_f s of 2.4 and 2.2 were found for soot from an Asian dust (AD) episode and a U.S. traffic source, respectively (Adachi, Chung, Friedrich, & Buseck, 2007). The electron tomography technique requires the 2D images from different projection angles to reconstruct the 3D object, which is a time-consuming process. Especially, since it is difficult to collect enough soot image samples from various projection angles, the 3D electron tomography method does not necessarily provide correct measurements for the fractal parameters. Therefore, the methods based on two-dimensional (2D) images are more commonly used (Brasil, Farias, & Carvalho, 1999; Köylü, Faeth, Farias, & Carvalho, 1995; Oh & Sorensen, 1997; Samson, Mulholland, & Gentry, 1987). Based on the 2D soot images, China, Mazzoleni, Gorkowski, Aiken, and Dubey (2013) found that the fractal dimension of ambient and denuded soot emitted from wildfires was 1.85 ± 0.05 and 1.53 ± 0.07 , respectively. While for soot particles at the freeway, the fractal dimensions were found to vary in the range of approximately 1.43 - 2.1 (China, Salvadori, & Mazzoleni, 2014). Yuan et al. (2019) showed that the D_f of bare-like soot, partly coated soot, and embedded soot at a remote site in the Southeastern Tibetan Plateau were 1.75 ± 0.08 , 1.82 ± 0.05 , 1.88 ± 0.05 , respectively. In the atmosphere, soot aggregates are commonly coated with other materials and the structures turn extremely complex (China et al., 2014; Wang et al., 2018, 2014; Yuan et al., 2019). Adachi et al. (2007), van Poppel et al. (2005) have demonstrated that the effects of monomer overlapping and inner pores hidden by the outer soot would affect the applicability of the 2D image analysis method, so the fractal parameters determined from 2D images are strongly influenced by the viewing point. However, the effects of coating materials are still unclear. For coated soot aggregates, many studies also analyzed the soot images based on the fractal law (China et al., 2013; Yuan et al., 2019), while for the atmospheric soot, the coating materials are difficult to completely remove from soot. Therefore, sometimes coating materials can be left on the soot during the measurement process. In many cases, the coated soot particle images are analyzed using the same method as the uncoated soot image analysis, and the soot outline depicted from the electron microscope images was commonly used for fractal analysis. However, as soot is coated with other materials (e.g. Organic carbon (OC)), it is difficult to see clearly the soot core, and the outline of soot depicted from the electron microscope images would include some coating materials. Therefore, the coating materials would affect the measured fractal parameters of soot particles. When using the 3D electron tomography method to analyze the morphologies of coated soot, as it is difficult to distinguish the soot core and coating materials from soot images, the calculated D_f should be the fractal dimension of coated soot. What is different about the 2D fractal analysis method? To see more deeply the different results produced between the 2D and 3D electron tomography methods, we revisit the most used 2D fractal analysis method.

The calculation of the fractal dimension of soot aggregates depends largely on the determination of N_s and R_g . In the 2D image analysis, N_s is determined by (Köylü et al., 1995; Oh & Sorensen, 1997; Samson et al., 1987):

$$N_s = k_a (\frac{A_a}{A_p})^{\alpha} \tag{3}$$

for freshly emitted fractal aggregates, where α is an empirical exponent and k_a is a constant; A_a and A_p are the projected area of the soot aggregate and the mean projected area of the soot monomer, respectively. R_g is calculated based on a relationship (Brasil et al., 1999):

$$\frac{L_{max}}{2R_g} = 1.50 \pm 0.05 \tag{4}$$

where L_{max} is the length of the longest dimension. Then D_f can be measured based on the slope of the following equation:

$$N_s = k_L \left(\frac{L_{max}}{d_s}\right)^{D_f} \tag{5}$$

where k_L is a scaling factor, and d_p represents the soot monomer's diameter measured from soot images.

In the above analysis, we notice that R_g is calculated based on L_{max} . For the coated soot in the atmosphere, in most cases, the coating materials commonly fill the voids among monomers firstly, so the L_{max} is close to that of the soot core. Therefore, the R_g measured from the 2D image analysis is close to that of the soot core. To understand the measured fractal dimension based on the 2D images, we need to figure out this question: If R_g of coated soot is close to that of the soot core, is the fractal dimension of coated soot also close to that of soot core? If it is, the measured fractal dimension based on the 2D images should be close to that of

the soot core, and this may be an important difference between the 2D method and the 3D electron tomography method for coated soot

Heinson, Liu, and Chakrabarty (2017) have concluded that the fractal dimension of the coated soot is close to that of the soot core, while the fractal prefactor increases with the coating thickness, and a simple analytical expression of the fractal prefactor was obtained:

$$k_0' = 1.34(\frac{a'}{a})^{1.7}$$
 (6)

where k'_0 represents the prefactor of coated soot; a and a' represents the monomer radius of the soot core and coated soot, respectively.

However, some numerical and experimental studies obtained different results (Lefevre, Yon, Bouvier, Liu, & Coppalle, 2019; Liu, Yon, & Bescond, 2016). Liu et al. (2016) found that the fractal dimension can increase as soot particles are coated. In the study of Heinson et al. (2017), coating materials were assumed to be uniformly coated on the soot cores, while in the atmosphere, soot particles are commonly unevenly coated, and the coating structures can vary in different conditions. Is the conclusion of Heinson et al. (2017) still satisfactory for the unevenly coated soot? What is the condition for the conclusion of Heinson et al. (2017)? Are the different conclusions for the coating-dependent fractal dimension in Heinson et al. (2017) and Liu et al. (2016) caused by the different coating structures? Previous studies have shown that the coating structures have a significant impact on the radiative properties of soot (Enekwizu, Singh, & Khalizov, 2020; Luo et al., 2019), while rather limited studies have investigated the effects of coating structures on the retrieval of fractal characteristics of soot. To answer the above questions, there is a need to further investigate the fractal characteristics of unevenly coated soot with different coating structures.

In this work, by investigating the variations of the fractal characteristics of soot particles as soot is coated, we aim to answer the following questions:

- 1. Can the fractal law still fit the morphology of unevenly coated soot?
- 2. What is the difference between the fractal dimension of coated soot determined using the 2D method and those determined using the 3D electron tomography method?
- 3. How do the fractal characteristics of soot particles change as soot is coated?

2. Methods

2.1. Generation of the simulated coated soot aggregates

Previous studies have shown that the diffusion-limited cluster aggregation (DLCA) aggregates can reflect the generation process of freshly emitted soot. The soot morphologies generated using the DLCA algorithm are greatly in agreement with the morphologies of freshly emitted soot (Sorensen & Feke, 1996; Sorensen & Roberts, 1997). However, in the atmosphere, soot can become more compact with atmospheric aging. Heinson et al. (2010) demonstrated that the morphology of soot aggregates can be well described by a (D_f, k_0) pair, so algorithms, where the fractal parameters are fully adjustable, were developed (Filippov, Zurita, & Rosner, 2000; Morán, Fuentes, Liu, & Yon, 2019; Skorupski, Mroczka, Wriedt, & Riefler, 2014; Woźniak, 2012), and these algorithms are referred to as the tunable algorithm. The tunable algorithm is commonly used to generate the fractal soot aggregates due to the fully adjustable parameters. Heinson et al. (2017, 2010) have further shown that the space-filling characteristics can be described by D_f , and k_0 can reflect the shape anisotropy. Even though the DLCA aggregates can more reflect the physical process of fresh soot generation, a tunable algorithm can reflect the structure of the DLCA aggregates by setting $D_f = 1.8$, $k_0 = 1.34$ (Heinson et al., 2017). So, the soot cores were generated using a tunable particle-cluster code developed by Woźniak (2012), which strictly satisfies the fractal law in each generation step. In this work, the monomer number varies from 1 to 600, which generally covers the observed range in the atmosphere. k_0 was fixed to be 1.34, which is consistent with the DLCA aggregates. D_f of 1.8, 2.2, 2.6 was considered to represent the soot from freshly emitted to aged. We must clarify that in real circumstances k0 can vary with the variation of D_f (Ehrl, Soos, & Lattuada, 2009; Morán et al., 2020). However, in this work, we are focused on how coating materials modify the fractal characteristics of soot, so we do not consider the variation of k_0 .

After soot cores were generated, coating materials were added on similar to our previous study (Luo et al., 2019). Here we briefly describe the algorithms used to add the coating materials. The 3D space was firstly discretized into high-resolution cubic lattices, and soot cores were placed in the simulation space, which resulted in the space being either filled with portions of the aggregate or left empty. Then the empty cubic lattices were filled with coating materials according to two coating methods. The first coating method determines the coating positions based on a tunable parameter, k. As shown in Figure S1, larger k can reflect more uniformly distributed coating materials. The second coating method determines the coating materials based on another tunable parameter, R_c , which is the radius of a defined sphere. The defined sphere generally reflects that most coating materials are distributed within the sphere, so the soot monomers within the sphere are more easily coated. By adjusting the R_c and the position of the center of the defined sphere, we can define the distribution of coating materials. In this work, the center of the defined sphere was located at the mass center of the soot core, and the coating morphology can become more spherical with the decrease of R_c . The generated soot morphologies are shown in Figure S2. The comparison of the generated soot morphologies and real soot morphologies are shown in Luo et al. (2019). For the details on the coating generation algorithms, please refer to Luo et al. (2019).

2.2. N_s versus R'_a/a' analysis

For uncoated soot, in a log-log axis of N_s versus R_g/a , the intercept and slope represent the fractal pre-factor and fractal dimension, respectively. For coated soot, even though the ideal fractal law can be inapplicable, to ensure consistency, similar to uncoated soot, we assumed that the intercept and slope in the log-log axis of N_s versus R_g'/a' represent the effective fractal pre-factor and fractal dimension, respectively. To figure out if the fractal law can describe the morphologies of coated soot, we used similar methods as the analysis of fractal structures. We defined the effective monomer radius (a') similar to the study of (Heinson et al., 2017):

$$\frac{V_{total}}{V_{core}} = \left(\frac{a'}{a}\right)^3 \tag{7}$$

where V_{total} and V_{core} are the volume of the total particle and soot cores, respectively.

We used soot volume fraction ($f_{soot} = V_{core}/V_{total}$) to represent the relative contents of soot and coating materials. As soot is coated, the effective monomer radius increases, and it would be polydisperse, so a' in Eq. (7) is just a mean monomer radius. We define an a' to represent the volume-mean monomer radius. For coated aggregates, a' becomes merely a formal parameter with little physical meaning due to an extensive overlap between the coatings centered on neighboring monomers.

To consider the effects of different coating structures, similar to Chakrabarty and Heinson (2018), the radius of gyration of coated soot aggregates (R'_a) was calculated based on the discretized cubic lattice:

$$R_g^{\prime 2} = \frac{1}{m_{total}} \left(\sum_{i=1}^{N_{ds}} \rho_{soot} V_d (\vec{R}_{ds,i} - \vec{R}_c)^2 + \sum_{i=1}^{N_{dc}} \rho_{coating} V_d (\vec{R}_{dc,j} - \vec{R}_c)^2 \right)$$
(8)

$$m_{total} = \sum_{i=1}^{N_{ds}} \rho_{soot} V_d + \sum_{i=1}^{N_{dc}} \rho_{coating} V_d$$

$$\tag{9}$$

$$\vec{R}_{center} = \frac{1}{m_{total}} \left(\sum_{i=1}^{N_{ds}} \rho_{soot} V_d \vec{R}_{ds,i} + \sum_{j=1}^{N_{dc}} \rho_{coating} V_d \vec{R}_{dc,j} \right)$$

$$\tag{10}$$

where m_{total} represents the total mass of soot-containing particles; V_d represents the volume of the discretized cubic lattice; N_{ds} and N_{dc} represent the number of discretized cubic lattices occupied by soot and coating materials, respectively. $\vec{R}_{ds,i}$ and $\vec{R}_{dc,j}$ represent the location of discretized cubic lattices occupied by soot and coating materials, respectively. \vec{R}_{center} represents the mass center of the soot-containing particle. ρ_{soot} and $\rho_{coating}$ represent the mass density of soot and coating materials, respectively.

For the mass density of soot, Horvath (1993) gave two typical values: $\rho_{soot} = 0.625 \text{ g/cm}^3$ and $\rho_{soot} = 1.125 \text{ g/cm}^3$. However, Janzen (1980) and Medalia and Richards (1972) pointed out that ρ_{soot} is approximately in the range of $1.8-1.9 \text{ g/cm}^3$, and Bergstrom (1972) suggested that ρ_{soot} is in the range of $1.9-2.1 \text{ g/cm}^3$. Bond and Bergstrom (2006) recommended us to use $1.7-1.9 \text{ g/cm}^3$. In order to reproduce the measured mass absorption cross-section, Kahnert (2010) recommended a ρ_{soot} value of $1.3-1.4 \text{ g/cm}^3$. In addition, Long, Nascarella, and Valberg (2013) further stated that the mass density of soot can vary from $1.2 \text{ to } 1.8 \text{ g/cm}^3$, so the measured ρ_{soot} value is in a wide range. We assumed that coating materials are mainly OC. The measurement range of the mass density of OC is also very wide. Turpin and Lim (2001) found that the mass density of OC in some areas near Los Angeles was 1.2 g/cm^3 , while the mass density of OC observed in the background was lower (0.87 g/cm³). By summarizing the literature, Turpin and Lim (2001) also found that the measured value of the OC mass density is usually in the range of 0.77 to 1.9 g/cm³. Therefore, the mass densities of OC and soot have an overlapping measurement range. Since this work mainly focuses on the overall structure of coated soot, we assume an identical mass density for soot and OC. However, considering that the mass density of soot and coating materials can be different in the atmosphere, we select the typical soot mass density (1.8 g/cm³) and OC mass density (1.2 g/cm³) for sensitivity analysis. In this work, it is assumed that the mass density of soot and OC are the same if without special description.

In this work, to see how the fractal characteristics vary as soot is coated, we used the methods for analyzing the fractal aggregates to analyze the morphologies of coated soot. However, the fractal law was just used to examine if the fractal law can fit the morphology of coated soot, and it does not mean that the fractal law can be applied to coated soot aggregates.

2.3. Q space analysis

The light scattering technique is widely used to infer the particle shape as it is significantly affected by the particle morphologies. Instead of plotting the scattered intensity versus the scattering angle, we can obtain a new perspective by plotting the scattered intensity versus the magnitude of the scattering wave vector with a log-log axis (Sorensen, 2013a, 2013b). Based on the Q space analysis, the scattering by particles with different shapes can be differentiated, and we can obtain a physical understanding of particle scattering from diffraction. The method has been applied to small-angle X-ray and neutron scattering for a long time, while it was not applied to the particle light scattering until approximately two decades ago (Sorensen & Fischbach, 2000). By revisiting the light scattering theory, a structure factor, S(q), was used to identify the q-space characteristics of the scattered intensity, as the Fourier transform of the real space structure (Berg, Sorensen, & Chakrabarti, 2005; Dobbins & Megaridis, 1987, 1991; Sorensen, 2013a; Sorensen & Shi, 2000).

For soot composed of N_d discretized cubic lattices, the scattering intensity (I(q)) can be expressed as (Cowley & Heydenreich, 1993; Warren, 1969):

$$I(q) = \sum_{i=1}^{N_d} \sum_{k=1}^{N_d} f_j f_k exp\left(i\vec{q} \cdot \left(\vec{R}_j - \vec{R}_k\right)\right)$$

$$\tag{11}$$

where f_j and f_k are the atomic scattering factor of the *j*th and *k*th lattice, respectively; \vec{R}_j and \vec{R}_k are the position of the *j*th and *k*th lattice, respectively.

S(q) can be expressed as I(q) normalized by $1/\sum_{i=1}^{N_d} f_i^2$ (Takeshi & Billinge, 2012):

$$S(q) = \frac{1}{\sum_{i=1}^{N_d} f_j^2} \sum_{j=1}^{N_d} \sum_{k=1}^{N_d} f_j f_k \exp\left(i\vec{q} \cdot \left(\vec{R}_j - \vec{R}_k\right)\right)$$
(12)

The magnitude of the scattering wave vector (q) is:

$$q = \frac{4\pi}{\lambda} \sin\left(\frac{\theta}{2}\right) \tag{13}$$

Recently, many studies have used the structure factor to analyze morphologies of uncoated fractal soot aggregates (Heinson, Heinson, Liu, & Chakrabarty, 2018; Heinson, Maughan, Heinson, Chakrabarti, & Sorensen, 2016; Lefevre et al., 2019; Liu et al., 2016; Sorensen, 2001). For uncoated soot, the slope of S(q) versus q is typically scaled by a power-law exponent of $-2D_m + D_s$ (where D_m is the mass dimension and D_s denote the surface dimension of the object). Specifically, for fractal aggregates, $D_f = D_m = D_s$, and $S(q) \propto q^{-D_f}$. Besides, Yon, Morán, Ouf, Mazur, and Mitchell (2021) demonstrated that S(q) is a function of the aggregate size. It is important to note that the above conclusion is only applicable for isotropic soot. In principle, to represent the light scattering intensity of coated soot, the atomic scattering factor of lattices occupied by soot core and coating materials should be different. However, if we consider the different optical properties of coating materials and soot, the structure factor is not only affected by the inner structure of coated soot but also the different optical properties of soot and coating materials, so the structure factor will not be applicable for the analysis of the fractal characteristics of coated soot. Nevertheless, this work is mainly focused on the overall structure of coated soot but not to measure the optical properties of coated soot. Therefore, we assumed that the atomic scattering factors of the soot core and coating materials are identical, and Eq. (12) can be simplified as:

$$S(q) = \frac{1}{N_d} \sum_{i=1}^{N_d} \sum_{k=1}^{N_d} \exp\left(i\vec{q} \cdot \left(\vec{R}_j - \vec{R}_k\right)\right)$$
 (14)

For isotropic soot, another form of Eq. (14) can be written as (Heinson et al., 2018; Sorensen, 2001):

$$S(q) = \frac{1}{N_d} \left| \sum_{i=1}^{N_d} exp\left(i\vec{q}.\vec{R}_j\right) \right|^2$$
 (15)

In the review of Sorensen (2001), S(q) was normalized to satisfy: S(0) = 1. However, to see clearer the q-space characteristics of soot aggregates with different monomers, we did not normalize S(q). In this work, the S(q) of coated soot with different coating structures was analyzed. However, as pointed by Heinson et al. (2017), we must clarify that the structure factor presented in this work is just for detecting the morphologies of coated soot but not a measure of optical properties.

3. Results and discussion

To see under what conditions the fractal law is applicable to coated soot and how the conclusion of Heinson et al. (2017) was obtained, we assumed that the structures of coated soot can be still fitted using an ideal fractal law:

$$N_s = k_0' \left(\frac{R_g'}{a'}\right)^{D_f'} = k_0' \left(\frac{R_g}{a} \cdot \frac{R_g'}{R_g} \cdot \frac{a}{a'}\right)^{D_f \cdot \frac{D_f}{D_f}}$$

$$\tag{16}$$

where R'_g represents the radius gyration of coated soot; D'_f and k'_0 represent the fractal dimension and fractal prefactor of coated soot, respectively.

Expanding the equation by substituting the R_g using Eq. (1), we can obtain

$$N_{s} = k_{0}' \left(\left(\frac{R_{g}}{a} \right)^{D_{f}} \right)^{\frac{D_{f}'}{D_{f}}} \cdot \left(\frac{R_{g}'}{R_{g}} \right)^{D_{f}'} \cdot \left(\frac{a}{a'} \right)^{D_{f}'} = k_{0}' \left(\frac{N_{s}}{k_{0}} \right)^{\frac{D_{f}'}{D_{f}}} \cdot \left(\frac{R_{g}'}{R_{g}} \right)^{D_{f}'} \cdot \left(\frac{a}{a'} \right)^{D_{f}'}$$
(17)

$$k'_{0} = N_{s}^{1 - \frac{D'_{f}}{D_{f}}} \cdot k_{0}^{\frac{D'_{f}}{D_{f}}} \cdot \left(\frac{R_{g}}{R'_{v}}\right)^{D'_{f}} \cdot \left(\frac{a'}{a}\right)^{D'_{f}}$$
(18)

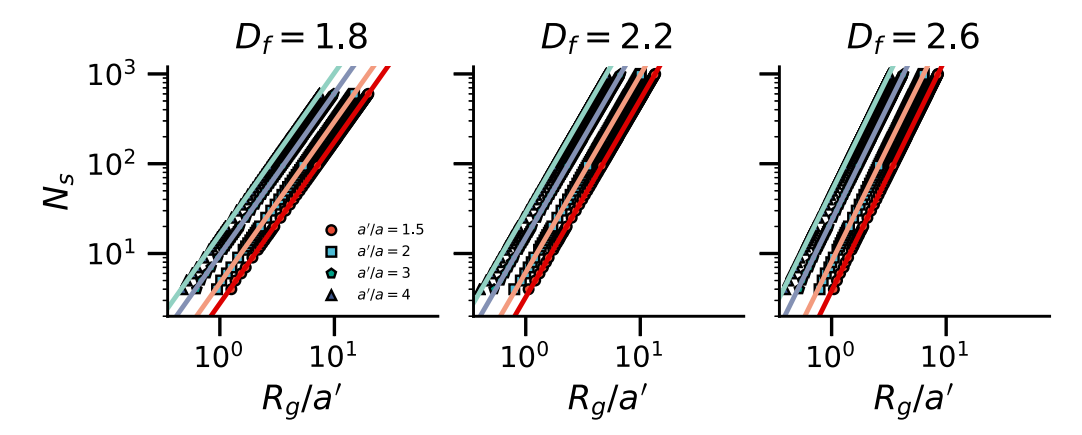


Fig. 1. The N_s versus R_g/a plot of coated soot if keeping R_r' unchanged, and the solid lines are fitted by Eqs. (22) – (23).

where the variation of $\frac{R_g'}{R_g}$ and $\frac{a'}{a}$ are caused by the increases of coating materials, and they are not directly related to N_s . If D_f' is not equal to D_f , k_0' varies with N_s , and the ideal fractal law is difficult to fit the morphology of coated soot aggregates. To obtain an ideal fractal law, we assumed D_f' to be D_f , so we can simplify the equation to be:

$$k_0' = k_0 \left(\frac{R_g}{R_g'}\right)^{D_f} \cdot \left(\frac{a'}{a}\right)^{D_f} \tag{19}$$

For the diffusion-limited cluster aggregation (DLCA) aggregates, k_0 and D_f are approximately 1.34 and 1.8, respectively. Therefore, we can obtain:

$$k'_0 = 1.34. \left(\frac{R_g}{R'_g}\right)^{1.8} \cdot \left(\frac{a'}{a}\right)^{1.8}$$
 (20)

Comparing Eq. (20) with the finding of Heinson et al. (2017), if $R'_g = R_g$, we can obtain:

$$k_0' = 1.34 \left(\frac{a'}{a}\right)^{1.8}$$
 (21)

Eq. (21) is similar to the results of Heinson et al. (2017). Therefore, the findings of Heinson et al. (2017) can be just applicable to the coated soot with a R'_g of close to R_g . In the study of Heinson et al. (2017), coating materials were assumed to be distributed uniformly on the soot surface, so the effective monomer centers are still close to that of the soot core. Thus, R'_g is close to the R_g of the soot core.

Furthermore, as Heinson et al. (2017) found that the fractal law can still fit the morphologies of coated soot, we guess that the fractal law can be applicable to the coated soot only when $R'_g = R_g$. If $R'_g = R_g$ and $D'_f = D_f$, we can obtain:

$$k_0' = k_0 \cdot \left(\frac{a'}{a}\right)^{D_f} \tag{22}$$

$$N_s = k_0' \left(\frac{R_g}{a'}\right)^{D_f} \tag{23}$$

To verify our guess, we firstly need to examine if the fractal law is applicable if we fix R'_g to be R_g . We firstly generated a group of soot cores using the tunable algorithm, and the R_g of each aggregate can be determined. Then we fixed the R_g of each aggregate, and just modified the monomer radius (a'), and the results are shown in Fig. 1. In Fig. 1, the lines were the fits (22) - (23). As shown in Fig. 1, the ideal fractal law described by Eqs. (22) - (23) can still fit the morphology of coated soot if $R'_g = R_g$.

To prove our guess, we also need to verify that the fractal law is inapplicable when R'_g is not equal to R_g . In the atmosphere, most soot aggregates are unevenly coated, and in most cases, R'_g is not equal to R_g . We applied the theory for fractal aggregates to analyze the morphologies of unevenly coated soot. In this work, R'_g was calculated based on the discretized cubic lattices. To validate the method for calculating the R'_g , we have calculated the R_g of uncoated soot using the method described in Eq. (8), and we plotted the power-law relationship of N_s versus R_g/a is not significantly modified when R_g is calculated using Eq. (8).

To analyze the fractal characteristics of coated soot aggregates, we plot the relationship of N_s versus R'_g/a' in a log-log axis. Fixing the soot volume fraction to be 75%, the fractal characteristics of coated soot with different coating structures are described in Fig. 2. With the first coating method, even with thin coating materials, the overall structure is difficult to be fitted by an ideal fractal law. Even though the structures of large coated soot can be still fitted by Eqs. (22) – (23), for the small coated soot aggregates, the

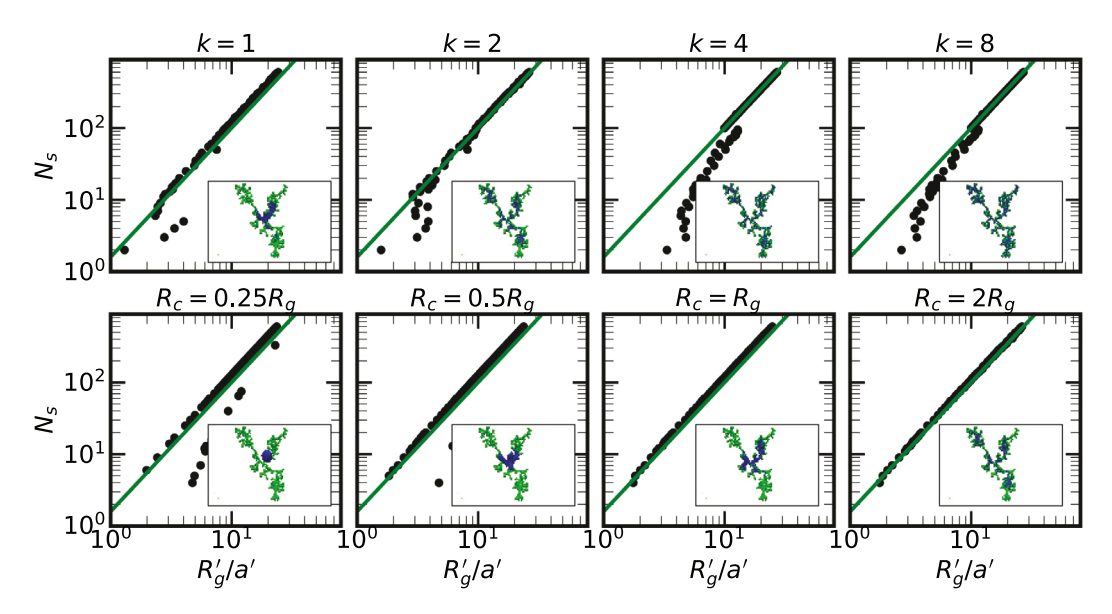


Fig. 2. N_s versus $\frac{K_s'}{a'}$ plot of thinly coated soot with a fluffy structure ($D_f = 1.8$), and the soot volume fraction is 75%. Rows 1 and 2 present soot with two different coating distributions. The insets of the figures represent typical simulated soot morphologies, and the green lines are fits to Eqs. (22) – (23). (For interpretation of the references to color in this figure legend, the reader is referred to the web version of this article.)

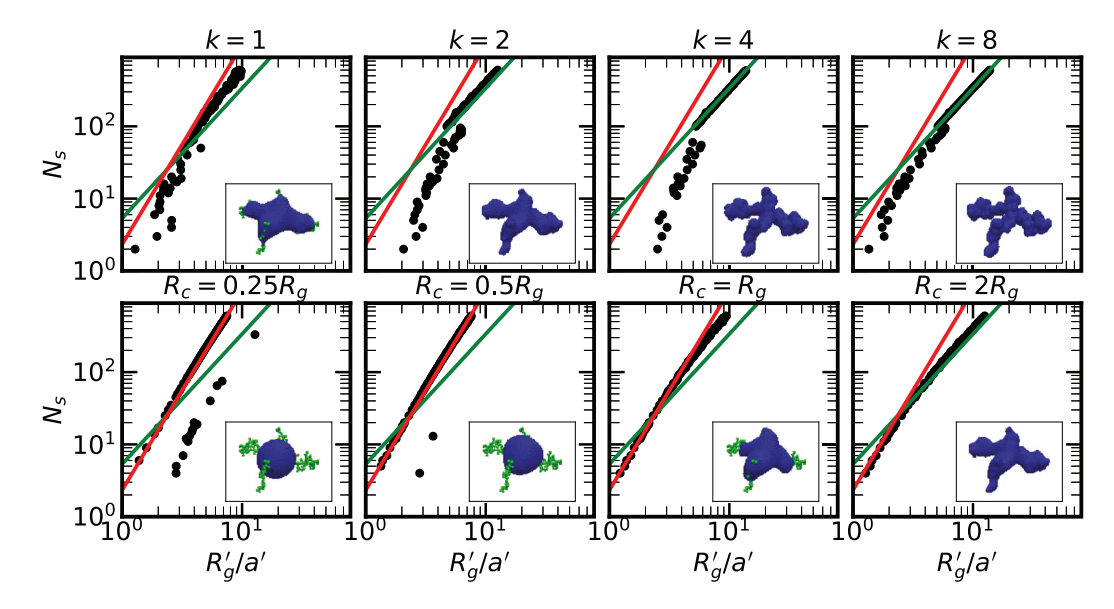


Fig. 3. Similar to Fig. 2, but for heavily coated soot, where the soot volume fraction is 10%. The green lines are fits to Eqs. (22) – (23), and the red lines are fits to the equation: $N_s = 2.33 \left(\frac{R_s}{a}\right)^{2.76}$. (For interpretation of the references to color in this figure legend, the reader is referred to the web version of this article.)

slope for the power-law of N_s versus R_g'/a' can be much steeper than 1.8 (the first coating method (k=4,8)), and the morphologies are difficult to be fitted using an ideal fractal law. With the second coating method, the fractal law described by Eqs. (22) – (23) can generally characterize the fractal characteristics of coated soot aggregates. The morphologies of coated soot can be well fitted by Eqs. (22) – (23) when R_c is large, while k_0' is a little larger than the values given by Eq. (22) when R_c is small, and the slope is a little larger than 1.8. Therefore, the coating structures would significantly affect the fractal characteristics of the fluffy, thinly-coated soot. In Fig. 2, some outliers were found in the data points. The reason may be that soot aggregates were unevenly coated in this work, and this may lead to some unconventional/extreme coating distributions.

Fig. 3 describes the fractal characteristics of heavily coated soot with different coating structures. Even though the fractal law described by Eqs. (22) – (23) can still fit the structures of large, heavily coated soot aggregates when the coating materials are distributed uniformly on the soot surface, the effective D_f' can increase as the coating structures become more spherical. Besides,

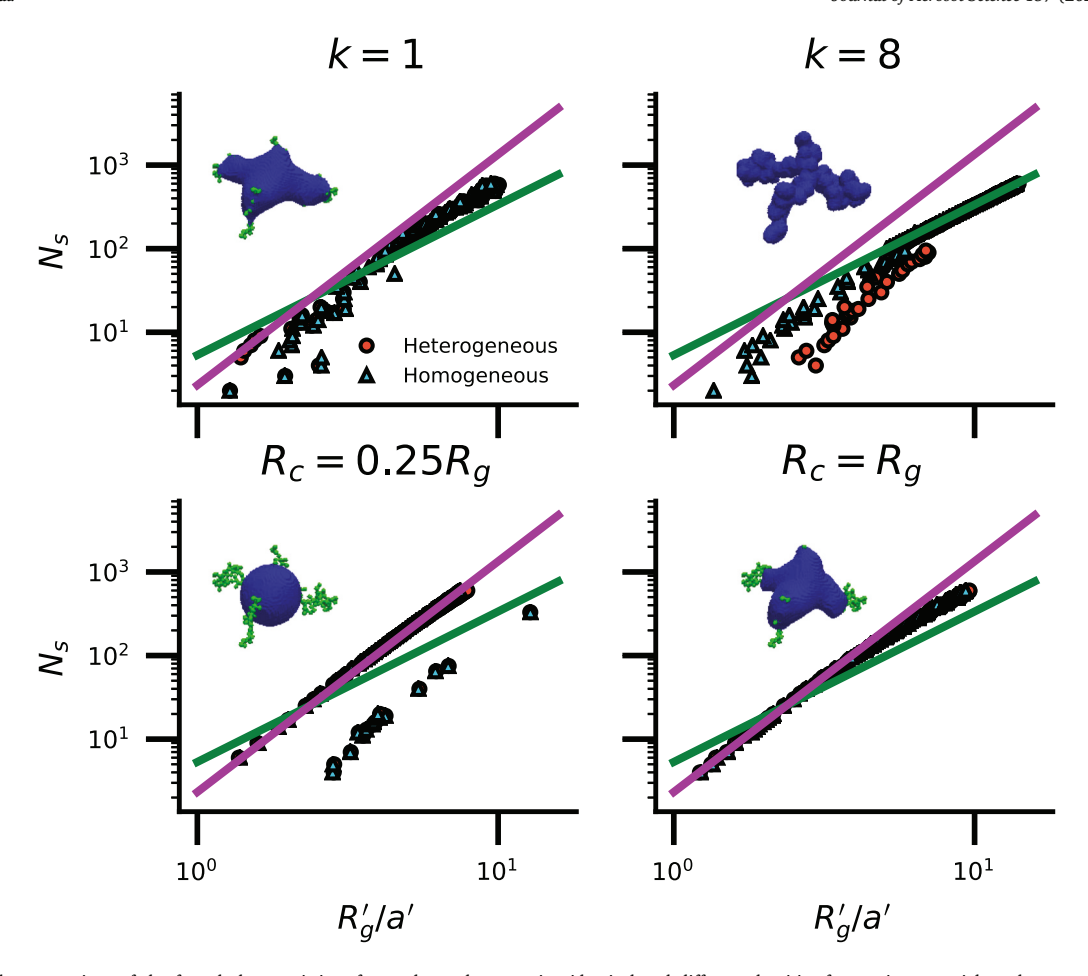


Fig. 4. The comparison of the fractal characteristics of coated soot by assuming identical and different densities for coating materials and soot, respectively, where $f_{soot} = 10\%$, $D_f = 1.8$, and the top and bottom rows reflect different coating distributions. The green lines are fits to Eqs. (22) – (23), and the violet lines are fits to the equation: $N_s = 2.33 \left(\frac{R_s}{a}\right)^{2.76}$. (For interpretation of the references to color in this figure legend, the reader is referred to the web version of this article.)

the ideal fractal law described by Eqs. (22) – (23) is difficult to fit the morphologies of small coated soot particles. As shown in Fig. 3, with the first coating method, Eq. (22) – (23) can generally fit the power-law of the large, heavily coated soot aggregates when k is large (k = 2, 4, 8), while the slope of the power-law can increase with decreasing k. However, with the second coating method, we noticed that the D_f' of heavily coated soot can increase. Fixing f_{soot} to be 10%, D_f' can reach approximately 2.76 and k_0' can reach approximately 2.33 when soot is with a nearly spherical coating structure ($R_c = 0.25 R_g$). As the coating materials is nearly uniformly distributed on the soot surface ($R_c = 2R_g$), the power-law relationship of N_s versus R_g'/a' for the structure of large, heavily coated soot is close to the analytical expression given by Eqs. (22) – (23), while for small coated soot, the effective D_f' and k_0' are still approximately 2.76 and 2.33, respectively. Besides, we notice that the effective fractal parameters of coated soot aggregates at different size scales can be varied, which means that the ideal fractal law is difficult to fit the morphologies of unevenly coated soot.

In the atmosphere, the densities of soot and coating materials can be varied. Fig. 4 shows the comparison of coating materials with the same mass density as the soot and those with different mass densities, and they were denoted as "Homogeneous" and "Heterogeneous", respectively. In the cases of "Heterogeneous", the mass density of soot and coating materials were assumed to be 1.8 g/cm^3 and 1.2 g/cm^3 , respectively. A similar conclusion can be drawn for the "Heterogeneous" case. As shown in Fig. 4, in most cases, the "Heterogeneous" densities of coating and soot do not significantly affect the fractal characteristics of coated soot, apart from k=8 for the first coating method, where some differences between the cases of "Homogeneous" and "Heterogeneous" were found when the unconventional coating distributions occur if soot particles are small. Therefore, the "Heterogeneous" densities do not affect the general conclusion of this work.

To make it convincing that the variation of the fractal dimension is mainly caused by the modification of R'_g , we have listed the R'_g of soot with different coating structures, as shown in Table 1. When N_s is small, R'_g is significantly affected by the coating materials, and this is why Eqs. (22) and (23) is difficult to fit the morphologies of small soot as soot is heavily coated, as shown in

Table 1 The radius of gyration of the soot core and heavily coated soot which is normalized using the monomer radius of the soot core (i.e. $R_{\rm g}/a$ for soot core and $R_{\rm g}'/a$ for coated soot). Here f_{soot} is assumed to be 10% for heavily coated soot. k=1 and k=4 represent the coated soot generated using the first coating method; $R_{\rm c}=0.25R_{\rm g}$ and $R_{\rm c}=R_{\rm g}$ represent the coated soot generated using the second coating method.

	Morphology	Soot core	Homogeneous	Heterogeneous
$N_s = 20$	k = 8	4.536825	5.818425	7.961292
	k = 1	4.536825	5.568964	5.532700
	$R_c = R_g$	4.536825	4.614015	4.611817
	$R_c = 0.25 R_g$	4.536825	8.579591	8.722327
$N_s = 100$	k = 8	11.010700	10.994286	11.662003
	k = 1	11.010700	9.041380	9.144889
	$R_c = R_g$	11.010700	8.595076	8.725983
	$R_c = 0.25 R_g$	11.010700	8.024328	8.191324
$N_s = 400$	k = 8	23.677540	23.640051	24.189559
	k = 1	23.677540	18.006886	18.318435
	$R_c = R_g$	23.677540	16.496689	16.909145
	$R_c = 0.25 R_g$	23.677540	13.642163	14.286373
$N_s = 600$	k = 8	29.777694	29.741317	30.175068
	k = 1	29.777694	20.384201	20.932547
	$R_c = R_g$	29.777694	20.130863	20.697245
	$R_c = 0.25 R_g$	29.777694	16.098404	17.012174

Fig. 4. If N_s is large enough ($N_s > 100$ in our cases), as coating materials are distributed uniformly on the soot surface (e.g. k = 8 for the first coating method), R'_g of coated soot is close to that of the soot core, so Eqs. (22) – (23) can still fit the morphologies of coated soot in that case (see Fig. 4). Nevertheless, as coating structures become more compact, R'_g of coated soot will deviate from the R_g of the soot core, which leads to the inapplicability of Eqs. (22) – (23).

In the atmosphere, soot aggregates would be collapsed to a compact structure with atmospheric aging. We have also analyzed the variation of fractal characteristics as the compact fractal soot aggregates are coated, and the results are shown in Figure S4–S7. Similar conclusions can be drawn for the compact soot aggregates. Differently, the D_f' of compact soot aggregates increases more easily after soot is coated, as the voids of more compact aggregates are more easily filled. For the soot core with $D_f = 2.6$, the D_f' of coated soot aggregates can reach approximately 2.9 even when the coating materials just account for 25% of the volume of the total particles, and the k_0' can increase to approximately 2.33. For the soot core with $D_f = 2.2$, unlike in the case of soot core with a D_f of 2.6, the D_f' of thinly coated soot is still close to 2.2 as it is more difficult to fill the voids for more fluffy soot. Combining the above analysis, we can conclude that the fractal law is just applicable for evenly coated soot where $R_g' = R_g$. For the unevenly coated soot, the ideal fractal law is difficult to fit the morphologies of coated soot. Besides, even though Eqs. (22) – (23) can still fit the morphology of the large, fluffy soot as the coating materials are distributed uniformly on the soot surface, the effective D_f' can increase as coating structures become more spherical, which is consistent with the findings of Liu et al. (2016). Furthermore, the effective D_f' can more easily increase for a more compact soot core.

To verify our findings, we have also calculated the structure factor S(q) by assuming the identical optical properties for soot core and coating. As shown in Figure S8, when the D_f of the uncoated soot is 1.8, 2.2, and 2.6, the slope of the power-law relationship of S_q versus q is -1.8, -2.2, and -2.6 respectively when q is smaller than approximately $2 \, \mu \text{m}^{-1}$, while the slope tends to approximately -4 if q is larger, which is consistent with the findings of previous studies (Heinson et al., 2017). However, as soot aggregates are coated, the structure factor is significantly modified. As shown in Figs. 5-6, for coated soot aggregates, the S(q) plot shows an earlier inflection to -4 power-law exponent as the soot aggregates are coated, which agrees with the findings of Heinson et al. (2017). As the -4 power-law exponent shows typical non-fractal particles, this finding shows the small coated soot does not present a fractal structure anymore. As the coating volume fraction increases to 90%, the global -4 power-law exponent can be observed, which means that the particles exhibit the characteristics of nearly spherical particles. For the DLCA aggregates, Heinson et al. (2017) showed that the relationship of S_q versus q for coated soot still exhibits a -1.8 power-law exponent before the inflection to -4, while some different results are found in this work. As shown in Fig. 6, for the aggregates with k=2,4,8 (the first coating method) and $R_c = 2R_g$ (the second coating method), the -1.8 power-law exponent can still well fit the relationship of S(q) versus q before the inflection. However, for other aggregates (such as $R_c = 0.25$ Rg with the second coating method), the slope is steeper than a -1.8 power-law exponent. By glancing at the generated soot images (see Fig. 3), we found that the coating materials are distributed nearly uniformly on the surface of soot when k=2,4,8 for the first coating method and $R_c=2R_o$ for the second coating method, so the coated soot still exhibits a fluffy structure. However, with k and R_c decreasing, the coated soot aggregates show more compact coating structures, and the slope can be steeper than a -1.8 power-law exponent. Therefore, the reason why a -1.8 power-law exponent was still observed by Heinson et al. (2017) is that the coating materials are not enough to fill the voids, and we believe the slope can be steeper as more coating materials are coated on. A similar phenomenon is found for more compact aggregates (See Figure S1–S4). Differently, the slope for the power-law of S(q) versus q is steeper than $-D_f$ even for aggregates with large k (k = 2, 4, 8 (the first coating method)) and large R_c ($R_c = 2R_g$ (the second coating method)) if the soot core is compact, as

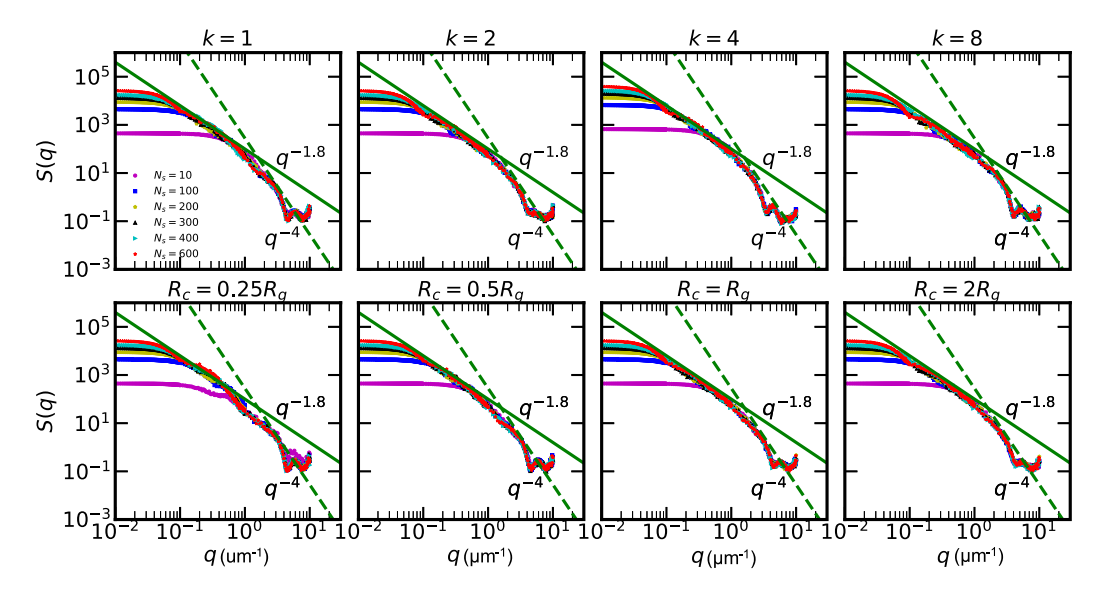


Fig. 5. Structure factor of thinly coated soot. The soot volume fraction is 75%, and the top and bottom rows reflect different coating distributions.

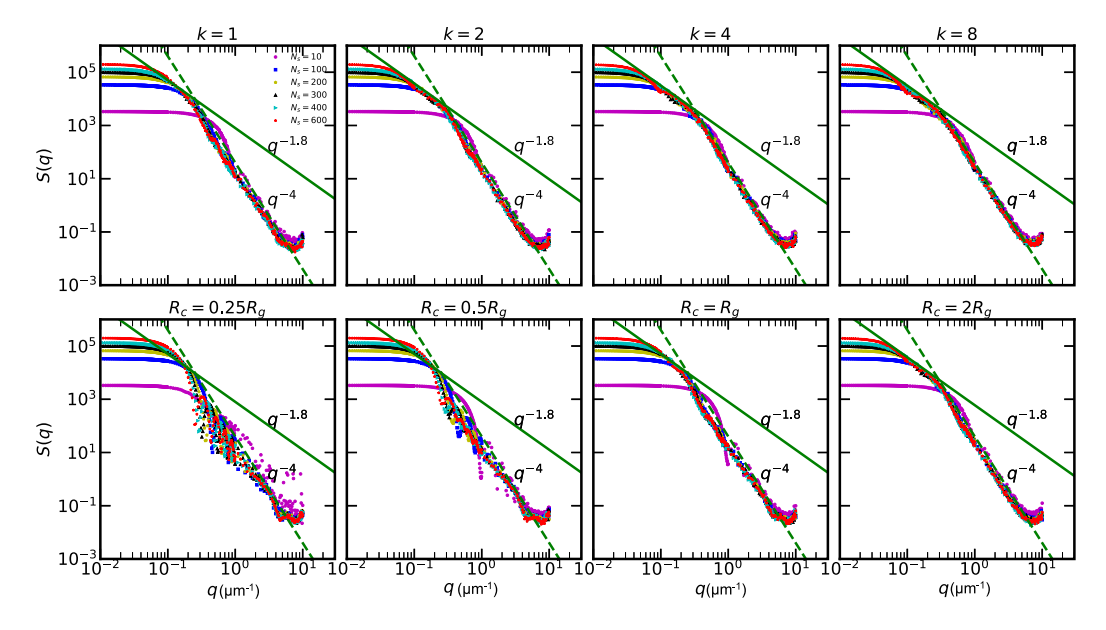


Fig. 6. Structure factor of heavily coated soot ($D_f = 1.8$). The soot volume fraction is 10%, and top and bottom rows reflect different coating distributions.

the voids of compact aggregates are more easily filled. Besides, the power-law exponent of S_q versus q is more easily increased to -4 for more compact soot cores.

4. Atmospheric implication

In this work, we found that the fractal law can apply to the coated soot only when $R'_g = R_g$. Besides, in that case, the fractal dimension of the coated soot is identical to that of the soot core. Our results can provide new insight into the different results produced between the 2D and 3D electron tomography methods. As described above, the R'_g calculated from the 2D soot images is close to the R_g of the soot core, and the fractal dimension is the same as that of the soot core if $R'_g = R_g$. Therefore, the fractal dimension of coated soot calculated using the 2D method should be close to that of the soot core. Even though d_p measured from the 2D image analysis is close to that of coated soot, it would just affect the k_0 , as we learn from Eqs. (22) – (23) and the findings of Heinson et al. (2017). On the other hand, the fractal dimension of coated soot calculated from the 3D electron tomography method is the fractal dimension of coated soot, which is larger than the fractal dimension of the soot core.

In the optical modeling, the D_f of soot cores is commonly assumed, then the coating materials are added on (Doner, Liu, & Yon, 2017; Kahnert, 2017; Kahnert, 2018; Liu & Mishchenko, 2018; Liu, Panetta, & Yang, 2012; Liu et al., 2016; Luo et al., 2019; Luo, Zhang, Wang and Zhang, 2018; Luo, Zhang and Zhang, 2018; Luo, Zhang, & Zhang, 2021; Luo et al., 2018). The optical modeling commonly requires the D_f of soot cores but not the D_f' of the overall coated soot structure. So, the use of the D_f of coated soot obtained using the 3D electron tomography method would be a little large for optical modeling, and the small D_f values analyzed using the 2D image analysis method are more preferred. However, we also notice that the 2D image analysis has some drawbacks. When the coating materials are distributed uniformly on the soot edge but do not fill the voids, the L_{max} is larger than that of the soot core, and the calculated D_f would be smaller than that of the soot core. Besides, the above 2D image analysis is just applicable for those aggregates with non-compact structure (D_f of the soot core is commonly less than 2.0) (China et al., 2015). Furthermore, the 2D method assumes that soot exhibit an ideal fractal structure, and some non-ideal minor structures can exhibit similar effects on the fractal characteristics of soot as coatings. For example, the effects of necking and overlapping should also be carefully considered (Doner et al., 2017).

5. Conclusions

Many studies have analyzed the atmospheric soot (including coated soot) based on the fractal law, and the coating materials are difficult to be completely removed during the measurements. Even though the structures of uncoated soot are widely accepted to be fitted greatly by the fractal law, the applicability of the fractal law to the coated soot is unclear. In this work, we have numerically investigated the variation of fractal characteristics as soot is coated. We found the ideal fractal law can provide great fits for the morphologies of coated soot only when the R'_g of coated soot is identical to that of the soot core, which can explain why an unchanged fractal dimension was observed by Heinson et al. (2017) as soot was evenly coated. Our results showed that even though Eqs. (22) – (23) can still fit the morphology of the large, fluffy coated soot as the coating materials are distributed uniformly on the soot surface, the effective fractal dimension can increase as the coating structures become more spherical, and the ideal fractal law is difficult to fit the structures of unevenly coated soot universally. The findings were also verified by Q-space analysis. As soot particles are unevenly coated, the global power-law exponent of S(q) versus q tends to -4 for heavily coated soot. This means that heavily, unevenly coated soot exhibits the characteristics of nearly spherical particles.

We also found that the D_f' of coated soot is the same as the D_f of the soot core if $R_g' = R_g$. As the voids of soot would be commonly filled firstly, the R_g' obtained from the 2D method is close to the R_g of the soot core. Therefore, the determined fractal dimension from 2D images would be close to that of the soot core. However, as coating materials are difficult to be completely removed from coated soot, the fractal dimension of atmospheric soot measured using the 3D electron tomography method is actually the fractal dimension of coated soot, which is larger than that of the soot core. In optical modeling, we commonly require the D_f of soot cores but not that of the overall structures, so D_f obtained from the 2D method is preferred.

Declaration of competing interest

The authors declare that they have no known competing financial interests or personal relationships that could have appeared to influence the work reported in this paper.

Acknowledgments

This work was financially supported by the National Natural Science Foundation of China (Grant 41675024 and No. U1733126); and the China Scholarship Council. Partial funding for the US authors was provided by the US National Science Foundation AGS division (AGS-1455215 and AGS-1926817). We also thank the support of the supercomputing center of the University of Science and Technology of China. The calculated data can be obtained from https://figshare.com/articles/dataset/The_fracteristics_of_coated_soot/12980300. We thank the constructive suggestions of three anonymous reviewers.

Appendix A. Supplementary data

Supplementary material related to this article can be found online at https://doi.org/10.1016/j.jaerosci.2021.105804.

References

Adachi, K., Chung, S. H., & Buseck, P. R. (2010). Shapes of soot aerosol particles and implications for their effects on climate. *Journal of Geophysical Research: Atmospheres*, 115(D15), http://dx.doi.org/10.1029/2009JD012868, arXiv:https://agupubs.onlinelibrary.wiley.com/doi/pdf/10.1029/2009JD012868 URL: https://agupubs.onlinelibrary.wiley.com/doi/abs/10.1029/2009JD012868.

Adachi, K., Chung, S. H., Friedrich, H., & Buseck, P. R. (2007). Fractal parameters of individual soot particles determined using electron tomography: Implications for optical properties. *Journal of Geophysical Research: Atmospheres*, 112(D14).

Berg, M. J., Sorensen, C. M., & Chakrabarti, A. (2005). Patterns in mie scattering: evolution when normalized by the Rayleigh cross section. *Applied Optics*, 44(34), 7487–7493.

Bergstrom, R. W. (1972). Predictions of the spectral absorption and extinction coefficients of an urban air pollution aerosol model. Atmospheric Environment (1967), 6(4), 247–258.

Bond, T. C., & Bergstrom, R. W. (2006). Light absorption by carbonaceous particles: An investigative review. Aerosol Science and Technology, 40(1), 27-67.

- Bond, T. C., Doherty, S. J., Fahey, D. W., Forster, P. M., Berntsen, T., DeAngelo, B. J., et al. (2013). Bounding the role of black carbon in the climate system: A scientific assessment. *Journal of Geophysical Research: Atmospheres*, 118(11), 5380–5552.
- Brasil, A., Farias, T. L., & Carvalho, M. (1999). A recipe for image characterization of fractal-like aggregates. Journal of Aerosol Science, 30(10), 1379-1389.
- Chakrabarty, R. K., & Heinson, W. R. (2018). Scaling laws for light absorption enhancement due to nonrefractory coating of atmospheric black carbon aerosol. Physical Review Letters, 121, Article 218701. http://dx.doi.org/10.1103/PhysRevLett.121.218701, URL: https://link.aps.org/doi/10.1103/PhysRevLett.121. 218701.
- Chakrabarty, R. K., Moosmüller, H., Arnott, W. P., Garro, M. A., Slowik, J. G., Cross, E. S., et al. (2007). Light scattering and absorption by fractal-like carbonaceous chain aggregates: Comparison of theories and experiment. *Applied optics*, 46(28), 6990–7006.
- China, S., Mazzoleni, C., Gorkowski, K., Aiken, A. C., & Dubey, M. K. (2013). Morphology and mixing state of individual freshly emitted wildfire carbonaceous particles. *Nature Communications*, 4(1), 1–7.
- China, S., Salvadori, N., & Mazzoleni, C. (2014). Effect of traffic and driving characteristics on morphology of atmospheric soot particles at freeway on-ramps. Environmental Science and Technology, 48(6), 3128–3135.
- China, S., Scarnato, B., Owen, R. C., Zhang, B., Ampadu, M. T., Kumar, S., et al. (2015). Morphology and mixing state of aged soot particles at a remote marine free troposphere site: Implications for optical properties. *Geophysical Research Letters*, 42(4), 1243–1250.
- Chỳlek, P., Ramaswamy, V., & Srivastava, V. (1983). Albedo of soot-contaminated snow. Journal of Geophysical Research: Oceans, 88(C15), 10837–10843.
- Cowley, J. M., & Heydenreich, J. (1993). Electron diffraction techniques (volume 1).. Crystal Research and Technology, 28(4), 560. http://dx.doi.org/10.1002/crat.2170280426, arXiv:https://onlinelibrary.wiley.com/doi/pdf/10.1002/crat.2170280426 URL: https://onlinelibrary.wiley.com/doi/abs/10.1002/crat.2170280426.
- Dobbins, R., & Megaridis, C. (1987). Morphology of flame-generated soot as determined by thermophoretic sampling. Langmuir, 3(2), 254-259.
- Dobbins, R. A., & Megaridis, C. M. (1991). Absorption and scattering of light by polydisperse aggregates. Applied Optics, 30(33), 4747-4754.
- Doner, N., Liu, F., & Yon, J. (2017). Impact of necking and overlapping on radiative properties of coated soot aggregates. *Aerosol Science and Technology*, 51(4), 532–542. http://dx.doi.org/10.1080/02786826.2016.1275513, arXiv:https://doi.org/10.1080/02786826.2016.1275513.
- Ehrl, L., Soos, M., & Lattuada, M. (2009). Generation and geometrical analysis of dense clusters with variable fractal dimension. *The Journal of Physical Chemistry B*, 113(31), 10587–10599. http://dx.doi.org/10.1021/jp903557m.
- Enekwizu, O., Singh, D., & Khalizov, A. (2020). Absorption and scattering of light by soot aggregates with uniform and pendular ring coatings. *Journal of Aerosol Science*, 147, Article 105583. http://dx.doi.org/10.1016/j.jaerosci.2020.105583, URL: http://www.sciencedirect.com/science/article/pii/S0021850220300720.
- Filippov, A., Zurita, M., & Rosner, D. (2000). Fractal-like aggregates: Relation between morphology and physical properties. *Journal of Colloid and Interface Science*, 229(1), 261–273. http://dx.doi.org/10.1006/jcis.2000.7027, URL: https://www.sciencedirect.com/science/article/pii/S0021979700970279.
- Forrest, S., & Witten, T., Jr. (1979). Long-range correlations in smoke-particle aggregates. Journal of Physics A: Mathematical and General, 12(5), L109.
- Forster, P., Ramaswamy, V., Artaxo, P., Berntsen, T., Betts, R., Fahey, D. W., et al. (2007). Changes in atmospheric constituents and in radiative forcing. Chapter 2. In Climate change 2007. the physical science basis.
- He, C., Flanner, M. G., Chen, F., Barlage, M., Liou, K.-N., Kang, S., et al. (2018). Black carbon-induced snow albedo reduction over the tibetan plateau: uncertainties from snow grain shape and aerosol-snow mixing state based on an updated SNICAR model. Atmospheric Chemistry and Physics (Online), 18(PNNL-SA-137623).
- Heinson, W. R., Heinson, Y. W., Liu, P., & Chakrabarty, R. K. (2018). Breakdown of fractal dimension invariance in high monomer-volume-fraction aerosol gels. Aerosol Science and Technology, 52(9), 953–956. http://dx.doi.org/10.1080/02786826.2018.1492086, arXiv:https://doi.org/10.1080/02786826.2018.1492086. Heinson, W. R., Liu, P., & Chakrabarty, R. K. (2017). Fractal scaling of coated soot aggregates. Aerosol Science and Technology, 51(1), 12–19.
- Heinson, Y. W., Maughan, J. B., Heinson, W. R., Chakrabarti, A., & Sorensen, C. M. (2016). Light scattering Q-space analysis of irregularly shaped particles. Journal of Geophysical Research: Atmospheres, 121(2), 682–691.
- Heinson, W., Sorensen, C., & Chakrabarti, A. (2010). Does shape anisotropy control the fractal dimension in diffusion-limited cluster-cluster aggregation?. Aerosol Science and Technology, 44(12), i-iv.
- Horvath, H. (1993). Atmospheric light-absorption a review. Atmospheric Environment Part A-General Topics, 27(3), 293–317.
- Janzen, J. (1980). Extinction of light by highly nonspherical strongly absorbing colloidal particles spectrophotometric determination of volume distributions for carbon-blacks. Applied Optics, 19(17), 2977–2985.
- Kahnert, M. (2010). On the discrepancy between modeled and measured mass absorption cross sections of light absorbing carbon aerosols. *Aerosol Science and Technology*, 44(6), 453–460.
- Kahnert, M. (2017). Optical properties of black carbon aerosols encapsulated in a shell of sulfate: comparison of the closed cell model with a coated aggregate model. Optics Express, 25(20), 24579–24593.
- Kanngießer, F., & Kahnert, M. (2018). Calculation of optical properties of light-absorbing carbon with weakly absorbing coating: A model with tunable transition from film-coating to spherical-shell coating. *Journal of Quantitative Spectroscopy and Radiative Transfer*, 216, 17–36.
- Köylü, Ü. Ö., Faeth, G., Farias, T. L., & Carvalho, M. d. G. (1995). Fractal and projected structure properties of soot aggregates. Combustion and Flame, 100(4), 621-633.
- Lapuerta, M., Martos, F. J., & Martín-González, G. (2010). Geometrical determination of the lacunarity of agglomerates with integer fractal dimension. *Journal of Colloid and Interface Science*, 346(1), 23–31.
- Lefevre, G., Yon, J., Bouvier, M., Liu, F., & Coppalle, A. (2019). Impact of organic coating on soot angular and spectral scattering properties. *Environmental Science and Technology*, 53(11), 6383–6391. http://dx.doi.org/10.1021/acs.est.8b05482.
- Liu, C., Li, J., Yin, Y., Zhu, B., & Feng, Q. (2017). Optical properties of black carbon aggregates with non-absorptive coating. *Journal of Quantitative Spectroscopy and Radiative Transfer*. 187, 443–452.
- Liu, L., & Mishchenko, M. I. (2005). Effects of aggregation on scattering and radiative properties of soot aerosols. *Journal of Geophysical Research: Atmospheres*, 110(D11).
- Liu, L., & Mishchenko, M. I. (2018). Scattering and radiative properties of morphologically complex carbonaceous aerosols: a systematic modeling study. *Remote Sensing*, 10(10), 1634.
- Liu, C., Panetta, R. L., & Yang, P. (2012). The influence of water coating on the optical scattering properties of fractal soot aggregates. Aerosol Science and Technology, 46(1), 31-43.
- Liu, F., Yon, J., & Bescond, A. (2016). On the radiative properties of soot aggregates part 2: Effects of coating. *Journal of Quantitative Spectroscopy and Radiative Transfer*, 172, 134–145. http://dx.doi.org/10.1016/j.jqsrt.2015.08.005, URL: http://www.sciencedirect.com/science/article/pii/S0022407315002800 Eurotherm Conference No. 105: Computational Thermal Radiation in Participating Media V.
- Liu, F., Yon, J., Fuentes, A., Lobo, P., Smallwood, G. J., & Corbin, J. C. (2020). Review of recent literature on the light absorption properties of black carbon: Refractive index, mass absorption cross section, and absorption function. *Aerosol Science and Technology*, 54(1), 33–51. http://dx.doi.org/10.1080/02786826. 2019.1676878, arXiv:https://doi.org/10.1080/02786826.2019.1676878.
- Long, C. M., Nascarella, M. A., & Valberg, P. A. (2013). Carbon black vs. black carbon and other airborne materials containing elemental carbon: Physical and chemical distinctions. *Environmental Pollution*, 181, 271–286.
- Luo, J., Zhang, Q., Luo, J., Liu, J., Huo, Y., & Zhang, Y. (2019). Optical modeling of black carbon with different coating materials: The effect of coating configurations. *Journal of Geophysical Research: Atmospheres*, 124(23), 13230–13253. http://dx.doi.org/10.1029/2019JD031701, arXiv:https://agupubs.onlinelibrary.wiley.com/doi/pdf/10.1029/2019JD031701
 URL: https://agupubs.onlinelibrary.wiley.com/doi/abs/10.1029/2019JD031701

- Luo, J., Zhang, Y., Wang, F., & Zhang, Q. (2018). Effects of brown coatings on the absorption enhancement of black carbon: a numerical investigation. Atmospheric Chemistry and Physics, 18(23), 16897–16914.
- Luo, J., Zhang, Y., & Zhang, Q. (2018). A model study of aggregates composed of spherical soot monomers with an acentric carbon shell. *Journal of Quantitative Spectroscopy and Radiative Transfer*, 205, 184–195.
- Luo, J., Zhang, Y., & Zhang, Q. (2021). Effects of black carbon morphology on the brown carbon absorption estimation: from numerical aspects. Geoscientific Model Development. 14.
- Luo, J., Zhang, Y., Zhang, Q., Wang, F., Liu, J., & Wang, J. (2018). Sensitivity analysis of morphology on radiative properties of soot aerosols. *Optics Express*, 26(10), A420–A432.
- Meakin, P. (1987). Fractal aggregates. Advances in Colloid and Interface science, 28, 249-331.
- Medalia, A. I., & Richards, L. W. (1972). Tinting strength of carbon-black. Journal of Colloid and Interface Science, 40(2), 233-&.
- Mishchenko, M. I., Dlugach, J. M., & Liu, L. (2016). Linear depolarization of lidar returns by aged smoke particles. Applied Optics, 55(35), 9968-9973.
- Morán, J., Fuentes, A., Liu, F., & Yon, J. (2019). Fracval: An improved tunable algorithm of cluster-cluster aggregation for generation of fractal structures formed by polydisperse primary particles. *Computer Physics Communications*, 239, 225–237. http://dx.doi.org/10.1016/j.cpc.2019.01.015, URL: https://www.sciencedirect.com/science/article/pii/S0010465519300323.
- Morán, J., Yon, J., Poux, A., Corbin, F., Ouf, F.-X., & Siméon, A. (2020). Monte Carlo Aggregation code (MCAC) part 2: Application to soot agglomeration, highlighting the importance of primary particles. *Journal of Colloid and Interface Science*, 575, 274–285. http://dx.doi.org/10.1016/j.jcis.2020.04.085, URL: https://www.sciencedirect.com/science/article/pii/S0021979720305336.
- Oh, C., & Sorensen, C. (1997). The effect of overlap between monomers on the determination of fractal cluster morphology. *Journal of Colloid and Interface Science*, 193(1), 17-25.
- van Poppel, L. H., Friedrich, H., Spinsby, J., Chung, S. H., Seinfeld, J. H., & Buseck, P. R. (2005). Electron tomography of nanoparticle clusters: Implications for atmospheric lifetimes and radiative forcing of soot. *Geophysical Research Letters*, 32(24), http://dx.doi.org/10.1029/2005GL024461, arXiv:https://agupubs.onlinelibrary.wiley.com/doi/pdf/10.1029/2005GL024461 URL: https://agupubs.onlinelibrary.wiley.com/doi/abs/10.1029/2005GL024461.
- Samson, R., Mulholland, G. W., & Gentry, J. (1987). Structural analysis of soot agglomerates. Langmuir, 3(2), 272-281.
- Schwarz, J., Spackman, J., Fahey, D., Gao, R., Lohmann, U., Stier, P., et al. (2008). Coatings and their enhancement of black carbon light absorption in the tropical atmosphere. *Journal of Geophysical Research: Atmospheres*, 113(D3).
- Skorupski, K., Mroczka, J., Wriedt, T., & Riefler, N. (2014). A fast and accurate implementation of tunable algorithms used for generation of fractal-like aggregate models. *Physica A. Statistical Mechanics and its Applications*, 404, 106–117. http://dx.doi.org/10.1016/j.physa.2014.02.072, URL: https://www.sciencedirect.com/science/article/pii/S0378437114001812.
- Sorensen, C. M. (2001). Light scattering by fractal aggregates: A review. Aerosol Science and Technology, 35(2), 648-687, URL: <GotolSI>://WOS: 000170467100003.
- Sorensen, C. (2013a). Q-space analysis of scattering by dusts. Journal of Quantitative Spectroscopy and Radiative Transfer, 115, 93-95.
- Sorensen, C. M. (2013b). Q-space analysis of scattering by particles: A review. *Journal of Quantitative Spectroscopy and Radiative Transfer*, 131, 3–12. http://dx.doi.org/10.1016/j.jqsrt.2012.12.029, URL: http://www.sciencedirect.com/science/article/pii/S0022407313000083 Concepts in electromagnetic scattering for particulate-systems characterization.
- Sorensen, C., & Feke, G. D. (1996). The morphology of macroscopic soot. *Aerosol Science and Technology*, 25(3), 328–337. http://dx.doi.org/10.1080/02786829608965399, arXiv:https://doi.org/10.1080/02786829608965399.
- Sorensen, C., & Fischbach, D. (2000). Patterns in mie scattering. Optics Communications, 173(1-6), 145-153.
- Sorensen, C. M., & Roberts, G. C. (1997). The prefactor of fractal aggregates. Journal of Colloid and Interface Science, 186(2), 447-452.
- Sorensen, C., & Shi, D. (2000). Guinier analysis for homogeneous dielectric spheres of arbitrary size. Optics Communications, 178(1-3), 31-36.
- Takeshi, E., & Billinge, S. J. (2012). Chapter 2 crystallographic analysis of complex materials. In T. Egami, & S. J. Billinge (Eds.), Pergamon materials series: Vol. 16, Underneath the bragg peaks (pp. 27–54). Pergamon, http://dx.doi.org/10.1016/B978-0-08-097133-9.00002-2, URL: https://www.sciencedirect.com/science/article/pii/B9780080971339000022.
- Turpin, B. J., & Lim, H.-J. (2001). Species contributions to PM2.5 mass concentrations: Revisiting common assumptions for estimating organic mass. *Aerosol Science and Technology*, 35(1), 602–610, arXiv:https://www.tandfonline.com/doi/pdf/10.1080/02786820119445.
- Wang, Q., Cao, J., Han, Y., Tian, J., Zhu, C., Zhang, Y., et al. (2018). Sources and physicochemical characteristics of black carbon aerosol from the southeastern tibetan plateau: internal mixing enhances light absorption. *Atmospheric Chemistry and Physics*, 18(7), 4639–4656. http://dx.doi.org/10.5194/acp-18-4639-2018, URL: https://acp.copernicus.org/articles/18/4639/2018/.
- Wang, Q., Huang, R.-J., Cao, J., Han, Y., Wang, G., Li, G., et al. (2014). Mixing state of black carbon aerosol in a heavily polluted urban area of China: Implications for light absorption enhancement. Aerosol Science and Technology, 48(7), 689–697. http://dx.doi.org/10.1080/02786826.2014.917758, arXiv:https://doi.org/10.1080/02786826.2014.917758.
- Warren, B. E. (1969). X-ray diffraction. Reading (Mass.): Addison-Wesley, URL: http://lib.ugent.be/catalog/rug01:000835542.
- Warren, S. G. (1982). Optical properties of snow. Reviews of Geophysics, 20(1), 67-89.
- Woźniak, M. (2012). Characterization of nanoparticle aggregates with light scattering techniques (Theses), Aix-Marseille Université, URL: https://tel.archives-ouvertes.fr/tel-00747711
- Yon, J., Morán, J., Ouf, F.-X., Mazur, M., & Mitchell, J. (2021). From monomers to agglomerates: A generalized model for characterizing the morphology of fractal-like clusters. *Journal of Aerosol Science*, 151, Article 105628. http://dx.doi.org/10.1016/j.jaerosci.2020.105628, URL: http://www.sciencedirect.com/science/article/pii/S0021850220301166.
- Yuan, Q., Xu, J., Wang, Y., Zhang, X., Pang, Y., Liu, L., et al. (2019). Mixing state and fractal dimension of soot particles at a remote site in the southeastern tibetan plateau. *Environmental Science and Technology*, 53(14), 8227–8234.